Hybrid Density Functional Theory Predictions of Low-Temperature Dimethyl Ether Combustion Pathways. II. Chain-Branching Energetics and Possible Role of the Criegee Intermediate

Amity Andersen and Emily A. Carter*

Department of Chemistry and Biochemistry, University of California, Los Angeles, Box 951569, Los Angeles, California 90095-1569

Received: May 22, 2003; In Final Form: August 7, 2003

In part I, we discussed the chain-propagating and possible competing mechanisms of low-temperature (300−1000 K) dimethyl ether (DME) combustion. Here we consider the chain-branching mechanism that results in explosive combustion, initiated by O_2 addition to the $\cdot CH_2OCH_2OOH$ intermediate formed in the earlier chain-propagation step. Ideally, chain-branching leads to the formation of two highly reactive ·OH radicals from the $\cdot OOCH_2OCH_2OOH$ precursor. Each of these two ·OH radicals can initiate a chain-reaction "branch" with another DME molecule, which, ideally, leads to the formation of four more ·OH, and so on. This exponential increase in ·OH concentration causes an exponential increase in the DME oxidation rate, leading to explosive combustion. Here we show that although the pathway to create the first ·OH from $\cdot OOCH_2OCH_2OOH$ in a hydrogen-transfer isomerization step is unambiguous, the formation of the second ·OH from the remaining hydroperoxyformate (HPMF or $HOOCH_2OC(=O)H$) fragment is potentially very complicated. HPMF has many possible fates, including $H\dot{C}O$ + formic acid ($HC(=O)OH$) + ·OH; H_2O + formic acid anhydride ($HC(=O)OC(=O)H$); the Criegee intermediate ($\cdot CH_2OO\cdot$) + formic acid; peroxyformic acid ($HC(=O)OOH$) + H_2 + CO; dihydroxymethylformate ($(HO)_2HCOC(=O)H$); $\cdot OCH_2OC(=O)H$ + ·OH; and quite possibly others. The first and last of these products derived from HPMF directly produce ·OH and thus can complete the chain-branching step. Activation energies of 42−44 kcal/mol are needed to overcome barriers to form these two sets of products from HPMF. While these pathways directly form ·OH, they may not be the most favorable. The formation of a Criegee intermediate ($\cdot CH_2OO\cdot$)−formic acid hydrogen-bonded adduct requires ∼15 kcal/mol less enthalpy than paths directly producing ·OH. Formation of the Criegee intermediate has never been considered as an intermediate in DME combustion before, but its formation (along with formic acid) appears to be the most favorable unimolecular path for HPMF decomposition. In atmospheric chemistry, decomposition of vibrationally excited $\cdot CH_2OO\cdot$ can potentially lead to ·OH formation. Thus, we propose $\cdot CH_2OO\cdot$ as a new intermediate that may significantly contribute to dimethyl ether's chain-branching mechanism.

I. Introduction

Dimethyl ether (DME) is a promising alternative diesel fuel because it readily compression ignites and produces little soot when burned. With the increasingly stringent environmental regulations being implemented by the U. S. Environmental Protection Agency,[1] DME has become an attractive potential alternative to the dirtier diesel fuels derived from fossil sources.[2] DME has other attractive attributes. Recently, one-step syntheses have been developed for cheaper production of DME from natural gas, syngas (and, in the future, biogas).[2] Moreover, the established liquid petroleum gas (LPG) technology could be utilized readily for a future DME storage and dispensing infrastructure.[2] DME also has the advantages of being nontoxic and photochemically inert (having been used as an aerosol propellant for years already).[2]

In Part I of this work, we analyzed the chain-propagation mechanism for DME combustion.[3] Though the focus of this article, Part II, is concerned only with chain-branching mechanisms (and competing pathways), we must emphasize that chain-branching in DME combustion hinges on the formation and lifetime of the $\cdot CH_2OCH_2OOH$ intermediate formed in the course of the chain-propagation mechanism. The first step of DME chain-branching is the addition of O_2 to $\cdot CH_2OCH_2OOH$. Thus we briefly summarize the chain-propagation steps leading to formation of $\cdot CH_2OCH_2OOH$.

The entire chain reaction mechanism starts with the abstraction of a hydrogen atom from the DME molecule by a highly reactive species (X) to form a methoxymethyl radical ($CH_3O\dot{C}H_2$):

$$CH_3OCH_2{-}H + X \rightarrow CH_3O\dot{C}H_2 + HX \qquad (1)$$

·OH is the most efficient species for the removal of a hydrogen atom from DME in a fuel/air mixture. O_2 and HOO· are also possible hydrogen abstractors, but are less efficient compared to ·OH.[4] O_2, in particular, is an important initiator in the degenerate branching mechanism proposed long ago by Semenov.[5] Though O_2 is much more abundant in the atmosphere compared with ·OH and is most likely to start the chain reaction, ·OH is much more reliable to sustain the chain reaction.

* Corresponding author. E-mail: eac@chem.ucla.edu.

10.1021/jp035423c CCC: $25.00
Published on Web 10/10/2003

Following the initiation step, O_2 adds to $CH_3O\dot{C}H_2$ at low temperatures to form a vibrationally-excited methoxymethyl peroxy radical ($CH_3OCH_2OO\cdot$*):

$$CH_3O\dot{C}H_2 + O_2 \rightleftarrows CH_3OCH_2OO\cdot^* \quad (2)$$

The fate of $CH_3OCH_2OO\cdot$ has three possible outcomes (at least on a short time scale), which resemble a Lindemann-type mechanism. $CH_3OCH_2OO\cdot$ may dissociate back into the reactants, $CH_3O\dot{C}H_2$ and O_2 (eq 2). $CH_3OCH_2OO\cdot$ can lose energy via collisions with a bath gas (indicated generically with a letter "M"):

$$CH_3OCH_2OO\cdot^* + M \rightarrow CH_3OCH_2OO\cdot + M \quad (3)$$

Finally, $CH_3OCH_2OO\cdot$ can undergo a chemical reaction to form products:

$$H-CH_2OCH_2OO\cdot^* \rightarrow \cdot CH_2OCH_2OOH \quad (4)$$

In the case of eq 4, $CH_3OCH_2OO\cdot$ isomerizes via an intramolecular hydrogen transfer to form $\cdot CH_2OCH_2OOH$. $\cdot CH_2OCH_2OOH$ can subsequently decompose into two formaldehyde molecules (CH_2O) and one $\cdot OH$:

$$\cdot CH_2OCH_2OOH \rightarrow 2CH_2O + \cdot OH \quad (5)$$

The pressure dependence of this mechanism has been demonstrated by Sehested et al.[6] in their smog chamber experiments at 296 K with a pressure range of 0.38−940 Torr. At the lowest pressures considered, they find formaldehyde to be the dominant product because there is a dearth of bath gas molecules available to collisionally stabilize $CH_3OCH_2OO\cdot$. At the high end of their pressure scale (940 Torr), self-reaction products methyl formate ($HC(=O)OCH_3$) and methoxymethylhydroperoxide (CH_3OCH_2OOH) are dominant because the $CH_3OCH_2OO\cdot$ has ample bath gas molecules available for collisional stabilization at 296 K. The laser-photolysis experiments by Maricq et al.[7] agree with the observations made by Sehested et al.[6]

However, pressure and temperature conditions in a diesel internal combustion engine far exceed conditions maintained in the experiments of Sehested et al.[6] and Maricq et al.[7] A few experimental studies have attempted to look at pressure and temperature conditions closer to that of a diesel engine and have shown that two-stage ignition occurs with increasing temperature. In particular, the shock-tube experiments of Pfahl et al.[8] use the most germane conditions, with pressures of 40 bar and a temperature range of 650−1300 K. Pfahl et al.[8] demonstrated that DME, like many long-chain alkanes, exhibits two-stage ignition with an "S"-shaped curve in an inverse temperature versus ignition delay time plot. Liu et al.[9] also observed two-stage ignition in their laminar flow experiments with FTIR analysis (but at atmospheric pressure). Liu et al. identified the stable products of these two stages of ignition. For the first stage, they find that formic acid ($HC(=O)OH$), formaldehyde, CO, and CO_2 are major stable products (from 513 to 713 K). For the second stage, stable products CO, CO_2, and CH_4 were observed.

Traditionally, an "S" curve outlines the transition between steady-state (e.g., chain-propagation) and explosive kinetics (e.g., chain-branching) in a temperature versus pressure plot.[4] By following an appropriate isobar from low to high temperatures, one observes first a transition from steady-state to explosive kinetics. This transition is attributed to chain-branching, which often results in a faint plume of chemiluminescence called a "cool-flame". The term "cool" implies that this so-called flame does not reach the adiabatic flame temperature, and, therefore, the fuel is not fully consumed in this brief "explosive" ignition stage. As the temperature rises from this burst of highly exothermic reactions, the system goes back into a steady-state "phase". During this phase the pool of reactive species continues to increase. When the temperature is high enough, the system then enters a second stage of explosive combustion. This time the explosive combustion is not due to chain-branching as it was in the previous low-temperature weakly explosive stage; it is due to a nonchain-branching source of highly reactive radicals such as that provided by the ~900 K breaking of the HO−OH bond in hydrogen peroxide (leading to two $\cdot OH$ for an exponential increase in the combustion rate),[4] formed from reactions in the interim steady-state stage between the low and high-temperature ignition stages. Kinetics modeling performed by Curran et al.[10,11] is sensitive to the following reactions in this interim stage, which can contribute to formation of HOOH:

$$H\cdot + O_2(+M) \rightarrow HOO\cdot(+M) \quad (6)$$

$$H\dot{C}O + O_2 \rightarrow CO + HOO\cdot \quad (7)$$

$$CH_2{=}O + HOO\cdot \rightarrow H\dot{C}O + HOOH \quad (8)$$

$$CH_3OCH_3 + HOO\cdot \rightarrow CH_3O\dot{C}H_2 + HOOH \quad (9)$$

This second stage of ignition leads to detonation of the remaining gas mixture, which leads to shock-waves. Of course, in an internal combustion engine, this second stage of hot ignition is undesirable because the shock-waves from fuel detonation can cause vibrational damage to the engine (this condition is called "knock"[12]). Engineering controls, such as the regulation of fuel injection into the combustion chamber to slowly make the fuel available for combustion, prevent the reaction from reaching this second stage of ignition.[13] However, the weaker "explosive" first stage of chain-branching reactions is crucial for the autoignition of a fuel in a diesel engine and is the focus of this work.

Kinetics simulations of the DME combustion mechanism conducted by Curran et al.[11] are the most extensive empirical modeling efforts to date and encompass observations from many experimental studies including those of Sehested et al.,[6] Maricq et al.,[7] Pfahl et al.,[8] Liu et al.,[9] and their own.[10,11,14,15] Here we outline the DME chain-branching mechanism proposed by Curran et al.[10,11] As stated above, chain-branching depends on the availability of $\cdot CH_2OCH_2OOH$; this chain-propagation intermediate is expected to have a long lifetime at low temperatures and high pressures (via bath gas collisional stabilization). Thus O_2 can collide with a fairly stable $\cdot CH_2OCH_2OOH$ to form $\cdot OOCH_2OCH_2OOH$:

$$\cdot CH_2OCH_2OOH + O_2 \rightleftarrows \cdot OOCH_2OCH_2OOH \quad (10)$$

Similar to $CH_3OCH_2OO\cdot$, $\cdot OOCH_2OCH_2OOH$ can undergo an intramolecular hydrogen-transfer isomerization to form $HOOCH_2O\dot{C}HOOH$:

$$\cdot OOCH_2OCH_2OOH \rightarrow HOOCH_2O\dot{C}HOOH \quad (11)$$

Finally, bond scission of the two O−O bonds on either end of $HO-OCH_2O\dot{C}HO-OH$ can yield two $\cdot OH$:

$$HO-OCH_2O\dot{C}HO-OH \rightarrow \cdot OCH_2OCHO + 2\cdot OH \quad (12)$$

Since eq 12 leads to two $\cdot OH$, rather than one $\cdot OH$ as in chain-

TABLE 1: Total Energies (UDFT-B3LYP) in Hartrees, Zero-point Vibrational Energy (ZPVE) in kcal/mol, and Thermal Corrections at 298 K in kcal/mol of Reactants, Intermediates, Transition States, and Products Relevant to the Branching Step of DME Combustion

	*6-31G***			*6-311G***		
species	total energy	ZPVE	*T* corr.[a]	total energy	ZPVE	*T* corr.[a]
branching path						
·CH_2OCH_2OOH (syn-chair)[b]	−304.720878	47.2	6.6	−304.805516	46.9	6.6
O_2[b]	−150.320021	2.4	2.1	−150.364775	2.3	2.1
·OH[b]	−75.728490	5.3	2.1	−75.754534	5.3	2.1
·$OOCH_2OCH_2OOH$ ("W")	−455.085716	53.1	8.4	−455.212313	53.0	8.4
·$OOCH_2OCH_2OOH$ ("helix")	−455.094552	53.4	8.2	−455.221506	53.3	8.3
·$OOCH_2OCH_2OOH$ ("ring")	−455.098276	54.1	7.9	−455.224389	53.9	7.8
b-TS1	−455.055056	49.7	8.6	−455.181310	49.6	8.6
$HOOCH_2OC(O)H\cdots OH$ [ap,ap]	−455.151960	51.0	9.3	−455.284784	51.2	9.3
$HOOCH_2OC(O)H\cdots OH$ [sp,ap]	−455.155163	51.2	9.3	−455.288112	51.2	9.2
$HOOCH_2OC(O)H$ [ap,ap]	−379.411328	44.1	6.9	−379.518485	43.9	6.9
$HOOCH_2OC(O)H$ [sp,ap]	−379.414757	44.2	6.8	−379.521996	44.0	6.8
$HOOCH_2OC(O)H$ [sp,sp]	−379.418894	44.8	6.6	−379.525728	44.6	6.6
b-TS2	−379.340154	39.3	7.7	−379.449142	39.1	7.7
HC(O)OH-*trans*	−189.762230	21.3	3.2	−189.819488	21.2	3.2
HC(O)OH-*cis*	−189.754125	21.1	3.3	−189.811319	21.0	3.3
$H\dot{C}{=}O$	−113.851840	8.2	2.5	−113.886608	8.1	2.5
·$OCH_2OC(O)H$	−303.609876	32.7	5.4	−303.694881	32.5	5.4
competing paths						
b-TS3	−379.328667	39.2	7.5	−379.439619	39.1	7.5
b-TS3′	−379.324222	39.3	7.6	−379.435646	39.1	7.6
HC(O)OC(O)H [sp,ap]	−303.080459	27.0	5.0	−303.166770	26.8	5.0
HC(O)OC(O)H [sp,sp]	−303.076012	26.8	5.0	−303.162581	26.6	5.0
HC(O)OC(O)H [ap,ap]	−303.075212	26.9	5.0	−303.161217	26.7	5.1
H_2O	−76.419759	13.4	2.4	−76.447466	13.4	2.4
b-TS4	−303.031930	23.8	5.5	−303.119670	23.6	5.5
CO	−113.309481	3.2	2.1	−113.346258	3.2	2.1
b-TS5	−379.341294	40.0	7.3	−379.449559	39.5	7.4
·CH_2OO·	−189.579922	19.6	3.4	−189.633445	19.5	3.4
$HC(O)OH\cdots CH_2OO$	−379.367403	42.0	7.2	−379.476922	42.1	7.2
b-TS6	−379.305206	37.6	7.8	−379.415643	37.3	7.8
H_2	−1.178540	6.4	2.1	−1.179571	6.3	2.1
HC(O)OOH-*cis*	−264.886339	23.4	4.3	−264.963275	23.3	4.3
HC(O)OOH-*trans*	−264.880622	22.8	4.6	−264.958137	22.8	4.6
b-TS7	−379.296670	38.4	7.9	−379.408484	38.0	8.0
$HC(O)OCH(OH)_2$	−379.514760	44.8	7.0	−379.625593	44.7	6.9

[a] Thermal correction calculated from constant-pressure heat capacities at 298 K obtained from the Jaguar code[21] using the formula $\int_0^{298} C_p dT$, where C_p is the heat capacity at constant pressure and T is the temperature. [b] These values are from Part I.[3]

propagation, chain-branching leads to an exponential increase in the rate of DME oxidation and, therefore, leads to explosive kinetics.

In this study, Part II, we use density functional theory with the Becke 3-parameter Lee−Yang−Parr (B3LYP) hybrid exchange-correlation functional to explore the potential energy surface of Curran et al.'s proposed chain-branching mechanism for DME autoignition, along with possible paths that may compete with chain branching. As we will see, the production pathway of one ·OH is trivial to ascertain, but the production of a second ·OH could involve a number of paths and may require indirect means for production. In particular, we find that the dihydroperoxy radical of eqs 11 and 12 is not stable, immediately losing the first ·OH to form a stable closed shell intermediate, hydroperoxymethyl formate (HPMF). The fate of HPMF is much more ambiguous, with several energetically accessible pathways to decomposition. These include, as we shall see, possible connections to atmospheric chemical reaction intermediates, namely the Criegee intermediate, ·CH_2OO·, which may be a source of the second ·OH required for explosive combustion.

II. Theoretical Method

The techniques used in this work are identical to those used in Part I (chain-propagation).[3] Total energies, optimized structures, and analytic harmonic frequencies for all reactants, intermediates, transition states (TS), and products relevant to the chain-branching path were performed using spin-polarized (unrestricted) density functional theory (UDFT).[61] The exchange-correlation functional chosen for these calculations (and the previous study on chain-propagation) is the hybrid Becke 3-parameter[16] with the Becke 88 GGA exchange functional[17] and the Lee−Yang−Parr[18,19] (B3LYP)[20] correlation functional. All DFT-B3LYP calculations were performed with the Jaguar v4.1 ab initio software package.[21] We used two basis sets for comparison: the 6-31G**[22−24] and the larger 6-311G**[25] basis set. Recent DFT-B3LYP and coupled-cluster with single and double excitations plus perturbative triple excitations (CCSD(T)) calculations performed by Schaefer and co-workers[26,27] for a similar system ($CH_3\dot{C}H_2 + O_2$) show that the performance of DFT-B3LYP is comparable to that of CCSD(T) (a method considered to give high-quality ab initio results).

For the transition state searches, we used the quadratic synchronous transit (QST) approach available in Jaguar.[21] The transition states presented in this work have only one imaginary harmonic frequency and therefore are genuine first-order transition states. The "Damped-Velocity-Verlet" (DVV) algorithm developed by Hratchian and Schlegel[28] was used to generate an approximate intrinsic reaction coordinate (IRC) to determine if the transitions found via QST actually connected to their

TABLE 2: Changes in the UDFT-B3LYP Total Energies (ΔE), Zero-Point-Corrected Enthalpies (ΔH_0), and Enthalpies Corrected to 298 K (ΔH_{298}) Relative to the Chain-Branching Reactants $\cdot CH_2OCH_2OOH + O_2$ for All Species Related to the Branching Path[a]

	*6-31G***			*6-311G***		
species	ΔE	ΔH_0	ΔH_{298}	ΔE	ΔH_0	ΔH_{298}
branching path						
$\cdot OOCH_2OCH_2OOH$ ("W")	−28.1	−24.6	−24.9	−26.4	−22.7	−23.0
$\cdot OOCH_2OCH_2OOH$ ("helix")	−33.7	−29.8	−30.2	−32.1	−28.1	−28.6
$\cdot OOCH_2OCH_2OOH$ ("ring")	−36.0	−31.4	−32.1	−33.9	−29.3	−30.0
b-TS1	−8.9	−8.7	−8.8	−6.9	−6.6	−6.7
$HOOCH_2OC(O)H\cdots OH$ [ap,ap]	−69.7	−68.2	−67.5	−71.8	−69.9	−69.4
$HOOCH_2OC(O)H\cdots OH$ [sp,ap]	−71.7	−70.0	−69.4	−73.9	−72.0	−71.5
$\cdot OH + HOOCH_2OC(O)H$ [ap,ap]	−62.1	−62.2	−61.9	−64.5	−64.5	−64.3
$\cdot OH + HOOCH_2OC(O)H$ [sp,ap]	−64.2	−64.3	−64.0	−66.7	−66.7	−66.5
$\cdot OH + HOOCH_2OC(O)H$ [sp,sp]	−66.8	−66.3	−66.3	−69.0	−68.4	−68.4
$\cdot OH$ + b-TS2	−17.4	−22.3	−21.2	−20.9	−25.8	−24.7
$2\cdot OH + HC(O)OH + H\dot{C}{=}O$	−18.9	−28.4	−27.3	−28.2	−37.5	−36.4
$2\cdot OH + \cdot OCH_2OC(O)H$	−16.3	−22.5	−21.7	−21.1	−27.3	−26.5
competing paths						
$\cdot OH$ + b-TS3	−10.2	−15.2	−14.3	−15.0	−19.9	−19.0
$\cdot OH$ + b-TS3′	−7.4	−12.4	−11.4	−12.5	−17.3	−16.4
$\cdot OH + HC(O)OC(O)H + H_2O$	−117.9	−121.7	−119.0	−124.5	−128.4	−126.9
$\cdot OH$ + b-TS4	−87.4	−94.5	−90.0	−95.0	−102.0	−98.8
$\cdot OH + HC(O)OH + CO + H_2O$	−112.4	−118.7	−117.7	−123.9	−130.1	−129.1
$\cdot OH$ + b-TS5	−18.1	−22.4	−21.7	−21.2	−25.7	−25.0
$\cdot OH + HC(O)OH + CH_2OO$	−18.7	−22.0	−22.0	−23.3	−26.6	−26.7
$\cdot OH + HC(O)OH\cdots CH_2OO$	−34.5	−36.7	−36.1	−38.4	−40.3	−39.7
$\cdot OH$ + b-TS6	4.5	−2.2	−1.0	0.1	−6.6	−5.4
$\cdot OH + H_2 + CO + HC(O)OOH$	−38.9	−50.2	−48.4	−46.0	−57.2	−55.4
$\cdot OH$ + b-TS7	9.9	4.0	5.3	4.6	−1.4	−0.1
$\cdot OH$ + DHMF	−127.0	−126.4	−126.1	−131.7	−131.0	−130.6

[a] All values are in kcal/mol. Thermochemistry for reactions involving species with more than one minimum conformation is calculated for the lowest-energy conformation.

intended reactants and products. This algorithm was implemented[29] in our pre-existing molecular dynamics code that employs the velocity Verlet algorithm.[30,31] We found that, for most of our transition states, the most stringent parameters used by Hratchian and Schlegel were not stringent enough: descent from the saddle point structures was often too rapid. Thus we used stricter parameters: $\upsilon_0 = 0.001$ bohr/fs (the constant velocity damping factor), $\Delta_0 = 0.003$ bohr (the error tolerance), and $0.025 \text{ fs} \leq \Delta t \leq 1.000$ fs (the time step constraint). For the initial "push" from the reaction coordinate for the DVV trajectories, we initialized velocities only along the reaction coordinate. We reversed the initial velocities along the transition state for a steepest descent into the opposite potential energy minimum. The descent into reactant and product minima typically took less than 2000 time steps. The only "problem" case was the descent from the saddle-point corresponding to the transition state for eq 11, which took 4000 time steps. The reason for this will be explained in the discussion.

III. Results and Discussion

Total energies (ΔE), zero-point vibrational energies (ZPVE), and heat capacities (C_p) at 298 K for chain-branching are shown in Table 1. Table 2 contains the thermochemistry for chain-branching (and possible competing) reactions derived from Table 1; thermochemistry in Table 2 is relative to $\cdot CH_2OCH_2OOH$ and O_2. The "b" label before the transition state label stands for "branching" to indicate the transition state is involved in (or competing with) the chain-branching mechanism (opposed to "p" for "propagating" as indicated in the previous paper, Part I[3]). The thermodynamic values for $\cdot CH_2OCH_2OOH$, O_2, and $\cdot OH$ appear in Part I.[3] All geometries in the ball-and-stick model figures showing the molecular geometries have bond lengths (in Å) and angles (in degrees) at the UB3LYP/6-311G** level

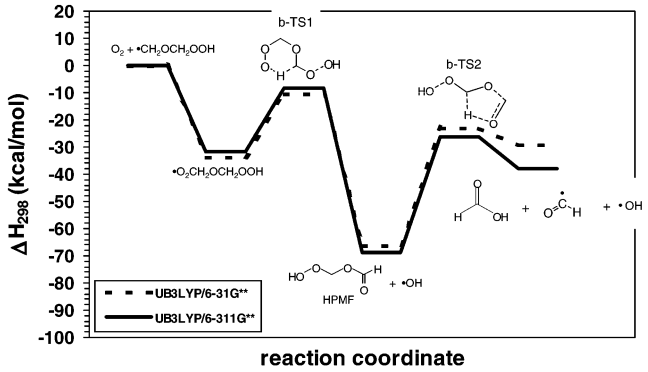

Figure 1. Possible chain-branching potential energy surface.

of theory. The color key for these figures is: white balls are hydrogens, light-gray balls are carbons, and dark-gray balls are oxygens. In the text, we report only the values for the 6-311G** basis.

A. Potential Energy Surface of Chain-Branching Reactions. The potential energy surface for the most efficient chain-branching path is shown in Figure 1. (By "most efficient" we mean efficiency in terms of direct production of two $OH\cdot$ via relatively low barriers.) Its beginning is similar to that of the chain-propagating path in that it commences with an O_2 molecule adding to a radical (in this case, $\cdot CH_2OCH_2OOH$); an H-transfer isomerization is also expected of the resulting $\cdot OOCH_2OCH_2OOH$ radical. The $\cdot OOCH_2OCH_2OOH$ radical is analogous to $CH_3OCH_2OO\cdot$ in that O_2 addition to $\cdot CH_2OCH_2$-OOH lacks a potential energy barrier and the resulting $\cdot OOCH_2$-OCH_2OOH is a stable intermediate, having sufficiently high barriers to reaction (via the reverse reaction of eq 10 and the reaction of eq 11). $\cdot OOCH_2OCH_2OOH$ has many more degrees of freedom than $CH_3OCH_2OO\cdot$; therefore, many more minimum-

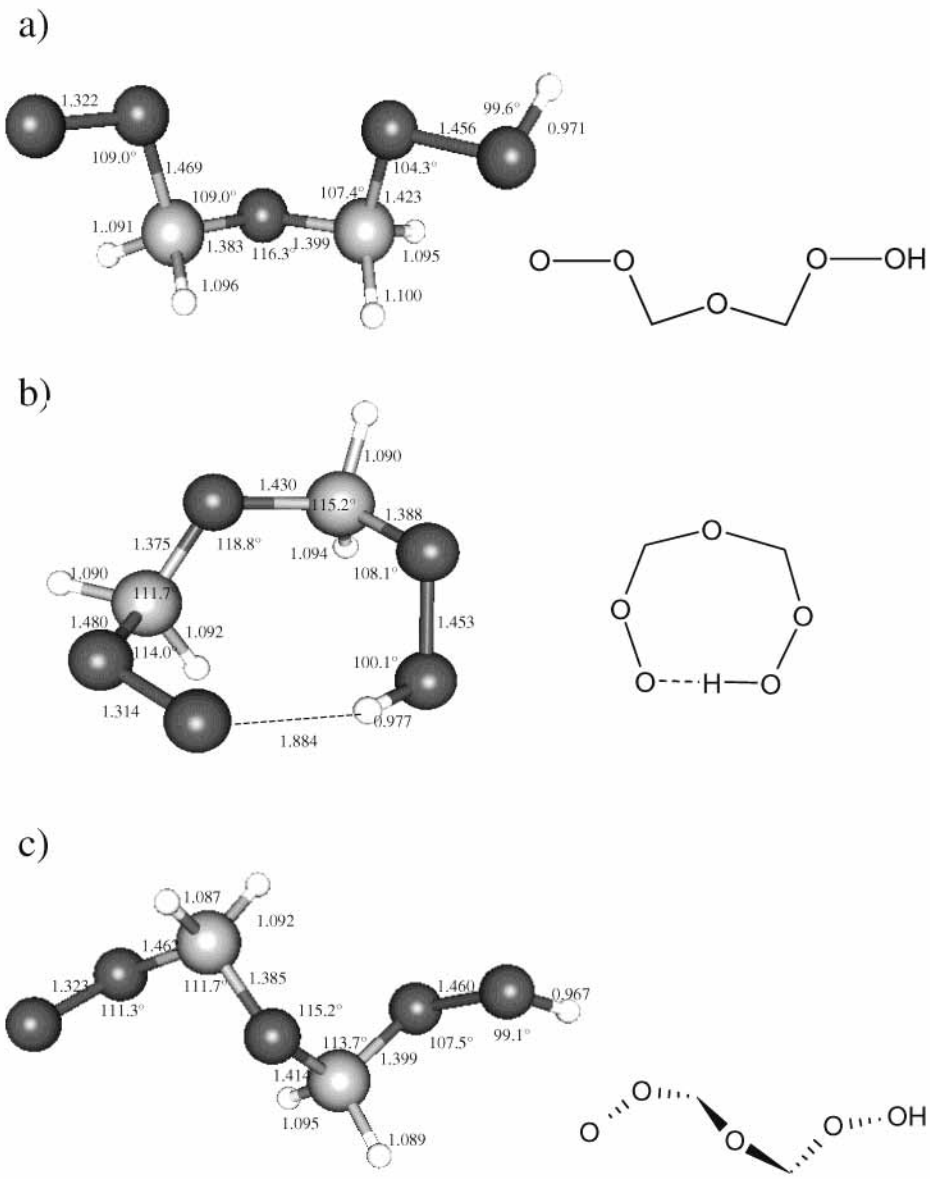

Figure 2. Representative conformations of $\cdot OOCH_2OCH_2OOH$: (a) "W", (b) "ring", and (c) "helix" conformations. Bond lengths given in Angstroms in all figures.

energy conformations are expected for $\cdot OOCH_2OCH_2OOH$. Figure 2 shows a small sample of the $\cdot OOCH_2OCH_2OOH$ minimum-energy conformations; though not complete, Figure 2 illustrates the diversity in the possible minima for $\cdot OOCH_2OCH_2OOH$. We name these sample structures according to the shape of their backbone. We shall call the structures of Figure 2 the (a) "W", (b) "ring", and (c) "helix" conformations, respectively. The lowest energy conformation is one in which the backbone forms a ring with an apparent tail-to-tail hydrogen bond interaction between the oxygen atom tail and the hydrogen atom tail (see Figure 2b; the H···O bond length is 1.884 Å). For this conformation, the enthalpy difference with respect to $\cdot CH_2OCH_2OOH$ and O_2 is $\Delta H_{298} = -30.0$ kcal/mol. These enthalpy differences are almost the same as those for the formation of $CH_3OCH_2OO\cdot$ (and even for the analogous $CH_3\dot{C}H_2 + O_2$ intermediate, $CH_3CH_2OO\cdot$[32]), characterized by the intrinsic exothermicity upon $R-O_2$ bond formation. With the many complex minimum energy structures of $\cdot OOCH_2OCH_2OOH$, reaction rates may depend on whether a given conformation can facilitate or hinder a chemical reaction. Further dynamics and kinetics studies may provide insight into the role of $\cdot OOCH_2OCH_2OOH$ in DME chain-branching kinetics.

Like $CH_3OCH_2OO\cdot$ produced by chain-propagation, $\cdot OOCH_2OCH_2OOH$ can either dissociate back into $\cdot CH_2OCH_2OOH$ and O_2 (reverse of eq 10), undergo collisional stabilization, or undergo an intramolecular hydrogen transfer isomerization (eq 11). The transition state leading to chain-branching via eq 11 (denoted b-TS1) is shown in Figure 3a. b-TS1 is connected on the reactant side by the lowest-energy ("ring") conformation of $\cdot OOCH_2OCH_2OOH$. This may provide a sterically favorable configuration by holding the shape of the molecule in such a way as to keep the two possible transferring hydrogens close to the oxygen atom tail of $\cdot OOCH_2OCH_2OOH$. Revisiting the $CH_3OCH_2OO\cdot$ complex discussed in Part I,[3] one could say that the lowest energy conformation (the "chairlike" conformation) is also sterically favorable since one of the three possible transferring hydrogens is also held in fairly close proximity to the oxygen tail end of $CH_3OCH_2OO\cdot$. The enthalpy difference of b-TS1 with respect to $\cdot CH_2OCH_2OOH$ is $\Delta H_{298} = -6.7$ kcal/mol. The corresponding activation barrier (at 298 K) with respect

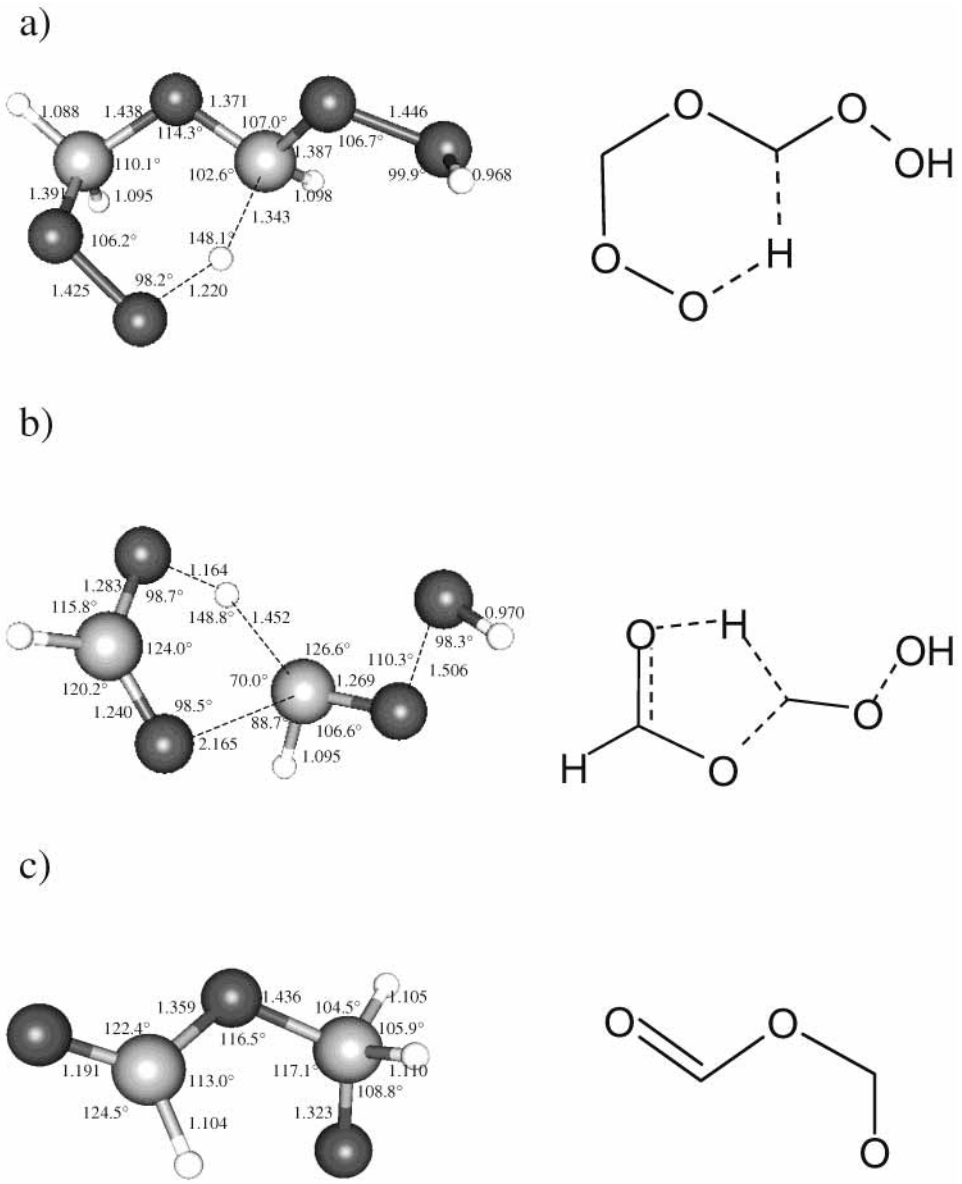

Figure 3. (a) b-TS1: connects $O_2CH_2OCH_2OOH$ ("ring") to HPMF [ap,ap]. Notation explained in section 3.1. (b) b-TS2: connects HPMF [sp,ap] to HC(═O)OH, HĊO, and ·OH. (c) ·OCH_2OCHO.

to the lowest energy ·$OOCH_2OCH_2OOH$ conformer is E_a = 23.3 kcal/mol. This may be compared with an 18.6 kcal/mol barrier derived from empirical group additivity estimates.[33]

After b-TS1 is surmounted, the resulting $HOOCH_2O\dot{C}HOOH$ formed is not a stable intermediate and promptly dissociates (without a potential energy barrier) into $HOOCH_2OC(=O)H$ (hydroperoxymethyl formate, or, simply, HPMF) and ·OH. Preliminary molecular dynamics trajectories initialized at b-TS1[29] show that $HOOCH_2O\dot{C}HOOH$ likely has a very short lifetime (50−100 fs). The prompt dissociation of $HOOCH_2O\dot{C}HOOH$ forms the first of two ·OH required for chain-branching.

Like ·$OOCH_2OCH_2OOH$, many potential energy minima exist for the $HO_2CH_2OC(=O)H$ intermediate. Though we found several minima, we show only three representative geometries in Figures 4a, b, and c. These fall into three categories, which are illustrated with the simplified two-dimensional chemical structures to the right of each of the three-dimensional structures in Figure 4: (1) structures that have all the oxygens in an "anti" configuration, (2) structures with the hydrogen atoms of the saturated carbon atom closest to the aldehyde oxygen atom, and (3) structures with the oxygens in a "syn" configuration. These three general groups of structures arise in part due to rotations about the C−O bond. Figures 4a, b, and c are shown in order of decreasing energy (i.e., increasing stability): the conformation of Figure 4a is higher by 2.2 kcal/mol than that of Figure 4b, which in turn is higher by 1.9 kcal/mol than that of Figure 4c. The stability trend correlates well with the number of H···O hydrogen-bonding interactions. In the lowest energy conformation (Figure 4c), the peroxide hydrogen and the aldehyde oxygen are only 1.838 Å apart, while the conformation in Figure 4a has the least H···O interactions. Figure 4b's conformation is between these two extremes. For structures similar to those shown in Figure 4, there are other possible O···H interactions such as attractions between the peroxide hydrogen and the ether oxygen, between the peroxide hydrogen and the aldehyde oxygen, etc. Such interactions tend to keep one of the hydrogens within ∼3 Å of one of the oxygens in HPMF in these conformations. The structure of Figure 4a is similar to that found in an earlier DFT-B3LYP calculations of Aplincourt and Ruiz-López.[34] As with the ·$OOCH_2OCH_2OOH$ conformations, the multitude of conformations of HPMF may affect its reaction

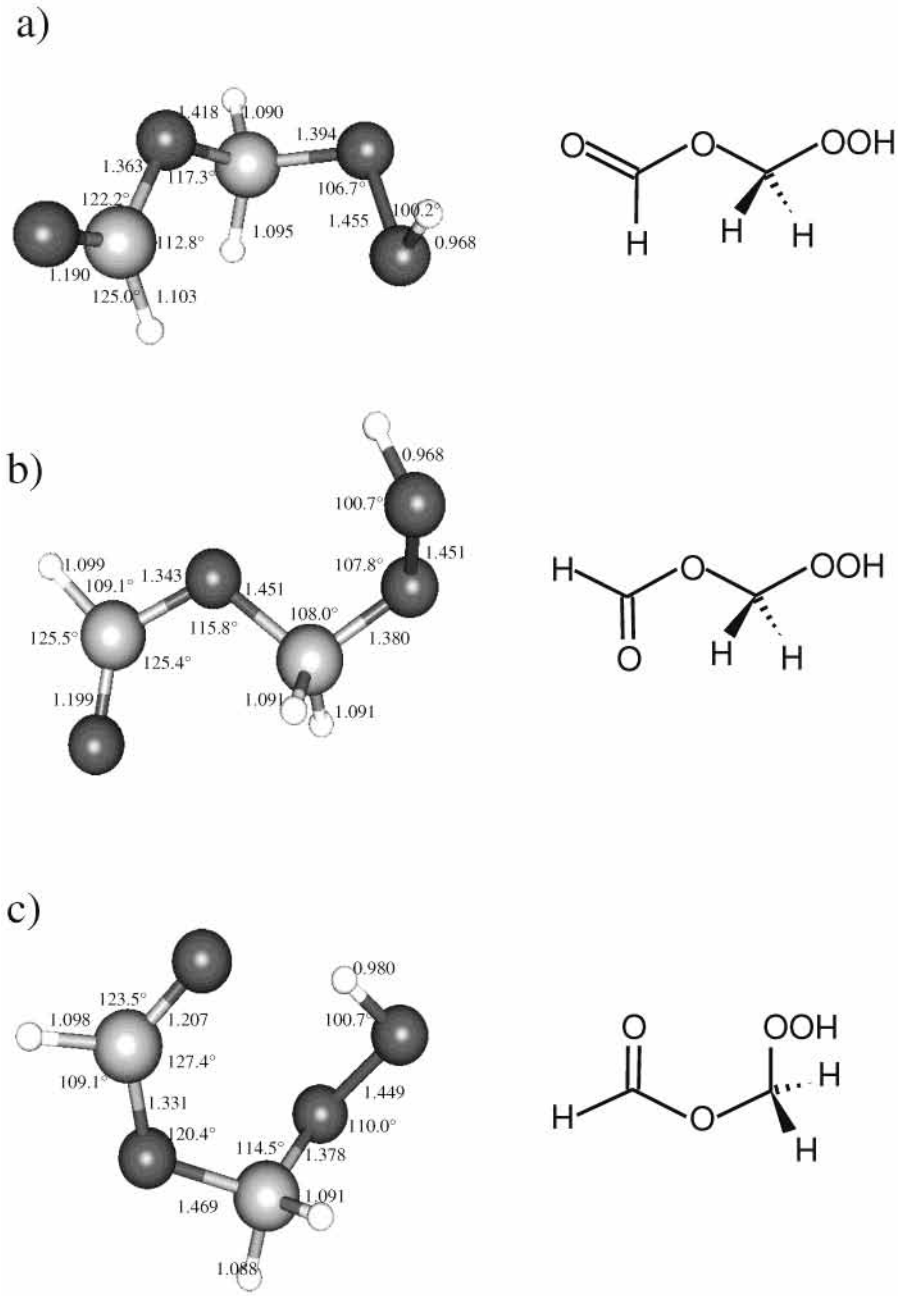

Figure 4. Hydroperoxymethyl formate (HPMF) primary conformations. These are defined with respect to the two O−C−O−C torsion angles. Note that many more conformations are possible if torsions along the O−O bond are considered; therefore, the following designations are approximate: (a) antiplanar, antiplanar [ap,ap]; (b) synperiplanar, antiplanar [sp,ap]; and (c) synperiplanar, synperiplanar [sp,sp].

kinetics and dynamics. Though it is not the lowest energy conformer, we find b-TS1 is connected on the product side to the structure of Figure 4a. The reaction $\cdot OOCH_2OCH_2OOH \rightarrow HOOCH_2OC(=O)H + \cdot OH$ is highly exothermic ($\Delta H^\circ_{rxn} = -38.4$ kcal/mol), with $\cdot OOCH_2OCH_2OOH$ ("ring") going to $HOOCH_2OC(=O)H\cdot\cdot\cdot OH$ [sp,sp].

Thus far, the chain-branching path proceeds uniquely to HPMF. By contrast, the decomposition path from $HOOCH_2OC(=O)H$ is ambiguous and may involve several paths prior to formation of a second ·OH. The transition states for $HOOCH_2OC(=O)H$ decomposition are all found to be at least 40 kcal/mol higher than $HOOCH_2OC(=O)H$. Thus $HOOCH_2OC(=O)H$ (a nonradical) can potentially have a significant lifetime if collisionally stabilized. However, many exothermic reactions have gone into the creation of $HOOCH_2OC(=O)H$ up to this point; therefore, $HOOCH_2OC(=O)H$ potentially possesses at least 70 kcal/mol of internal energy, making vibrational relaxation of this molecule very difficult, thereby allowing access to decomposition pathways with locally high barriers. Indeed, Liu et al.[9] noted that they do not detect the appearance of $HOOCH_2OC(=O)H$ in the FTIR spectra of their DME combustion experiments (even at room temperature). They cited the work of Thamm et al.[35] who synthesized HPMF through ozonolysis of ethyl vinyl ether and reported that their isolated HPMF has a half-life of 35 min at room temperature (in the gas phase), which is more than a sufficient amount of time for FTIR detection; therefore, Liu et al. expected to be able to detect the formation of HPMF in their experiments. Liu et al.'s experiments[9] pertain to low-temperature (513−973 K) DME combustion where HPMF has the potential to be formed with a large amount of internal energy. On the other hand, Thamm et al.'s experiments[35] are room temperature ozonolysis

experiments where HPMF is likely formed from HC(═O)OH addition to ·CH_2OO· and therefore HPMF would have less internal energy compared with HPMF formed in Liu et al.'s experiments. Thus Liu et al. may not have seen HPMF because their HPMF, having a much higher internal energy than that created in Thamm et al.'s experiments, dissociated too quickly to be detected. Chain-branching in DME combustion is expected to reach a peak rate around 600 K at 1 atm,[9,11] and therefore the decomposition of HPMF may involve other reaction paths at temperatures twice that of Thamm et al.'s experiments. Thamm et al.[35] noted that at room temperature, HPMF eventually dissociates into HC(═O)OH (formic acid), formic acid anhydride (FAA), and CH_2═O. This suggests a dehydration of HPMF. FAA is not thermally stable and decomposes into formic acid and CO. Liu et al.[9] observe formic acid as one of the products of room-temperature DME combustion, but HPMF dehydration may not be the source of formic acid in their experiments. Curran et al.[11] also observed in their Princeton Flow Reactor Study a relatively large concentration of formic acid at low temperatures.

Here we consider paths leading directly to the formation of the second ·OH needed for chain-branching, in order of increasing activation barriers. This can be accomplished via H-atom transfer surmounting b-TS2 (see Figure 1 and Figure 3b). In addition to ·OH, this path leads to direct formation of formic acid, HC(═O)OH (a major product observed in the combustion of DME by Liu et al.[9]) and HĊ═O. Curran et al.[11] predicted via kinetics modeling and sensitivity analysis that the latter species may be a major intermediate in the temperature range between the chain-branching and non-chain-branching stages of ignition (see eq 7). b-TS2 involves a transfer of one of the two hydrogen atoms from the saturated carbon atom of $HOOCH_2OC$(═O)H to the aldehyde oxygen. The decomposition of $HOOCH_2OC$(═O)H through b-TS2 into HC(═O)OH, HĊ═O, and ·OH appears to be concerted (i.e., HC(═O)OH, HĊ═O, and ·OH are formed almost at the same time). This mechanism via b-TS2 was originally proposed by Curran et al.[11] The transition state (b-TS2) is exothermic relative to ·CH_2OCH_2OOH + O_2 by $\Delta H_{298} = -26.3$ kcal/mol, while the activation energy (at 298 K) with respect to the lowest energy $HOOCH_2OC$(═O)H conformer (Figure 4b) is $E_a = 43.7$ kcal/mol.

Curran et al.[11] have argued that a transition state like b-TS2 involving this type of hydrogen transfer would not be a likely mechanism because a b-TS2 type transition state would have a small A-factor (frequency factor) due to its tight structure. For five- and six-centered transition states leading to decomposition products, estimated A-factors range from $10^{11.5}$ to 10^{15} s^{-1};[36] preliminary estimates of the kinetics calculated with RRKM theory and standard transition state theory indicate that the A-factor for b-TS2 is on the high end of this range ($10^{14}-10^{15}$ s^{-1}).[29] This is expected, since the products resulting from the reaction through b-TS2 are only about 7−11 kcal/mol below the transition state. Therefore, b-TS2 is product-like (Hammond's postulate) and fairly loose. Also, since this is a concerted reaction where the C−O bond breaks along with a hydrogen transfer, b-TS2 is looser than an isomerization reaction like that through b-TS1 (which has an estimated $10^{13}-10^{14}$ s^{-1} A-factor).[29] Simple bond-scission reactions to radical products (such as the O−O simple scission in HPMF to OCH_2OC(═O)H favored by Curran et al.[11]) have even looser transition states (with no well-defined saddle-point structure) and tend to have larger A-factors ($10^{16}-10^{17.5}$) than the five- and six-centered transition states.[36] Interestingly, high-pressure A-factors for similar reactions such as HO−OH, CH_3O−OH, and CH_3CH_2O−OH scissions, reported by Baulch et al.,[37] are actually rather low (3×10^{14}, 4.0×10^{15}, and 4.0×10^{15}, respectively). High-pressure A-factors reported by Sahetchian et al. for large peroxides[38] such as those of *tert*-butylO−OH, 1-heptylO−OH, and 2-heptylO−OH are on, or slightly lower than, the low-end of the typical simple scission A-factor range (5.0×10^{15}, 1.3×10^{16}, and 7.9×10^{15}, respectively). Considering A-factors alone, O−O bond scission in HPMF may have a higher rate to dissociation than the path to direct ·OH production through b-TS2. However, for a case such as this with no well-defined saddle-point structure, a full variational transition state theory (VTST) treatment is needed to determine the true rate constant. b-TS2 may yet turn out to be competitive as a result.

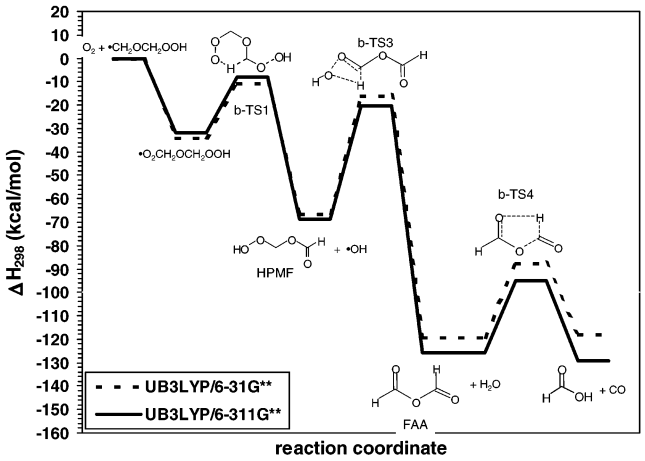

Figure 5. Potential energy surface for the dehydration of HPMF.

As mentioned above, Curran et al. favor $HOOCH_2OC$(═O)H dissociating directly into ·OH and ·OCH_2OC(═O)H (Figure 3c). We find that ·OCH_2OC(═O)H is a stable intermediate, with $\Delta H_{298} = 26.5$ kcal/mol below O_2 + ·CH_2OCH_2OOH. The O−O bond energy in HO−OCH_2OC(═O)H is $D_{298} = 41.9$ kcal/mol (with respect the lowest-energy $HOOCH_2OC$(═O)H conformer), weaker than the analogous bonds in HO−OH ($D_{298} = 51.3$ kcal/mol[39]), CH_3O−OH ($D_{298} = 46.6$ kcal/mol[37]), CH_3CH_2O−OH ($D_{298} = 43.0$ kcal/mol[37]), and 1-heptylO−OH ($D_{298} = 44.0$ kcal/mol[38]), but comparable to those in *tert*-butylO−OH ($D_{298} = 40.6$ kcal/mol[38]) and 2-heptylO−OH ($D_{298} = 41.6$ kcal/mol[38]). Therefore, the O−O bond in HPMF is likely to rupture at a lower temperature than those in HOOH, CH_3OOH, CH_3CH_2-OOH, and 1-heptylOOH, but at temperatures comparable to those needed to break the O−O bonds in *tert*-butylOOH and 2-heptylOOH. The HO−OCH_2OC(═O)H bond-breaking process appears not to have a potential energy barrier beyond its endothermicity (i.e., no transition state was found), suggesting this pathway may be competitive with the path via b-TS2.

B. Competitors to the Chain-Branching Path. *1. Formation of Formic Acid Anhydride, Formic Acid, CO, and H_2O: Dehydration of Hydroperoxymethyl Formate.* As mentioned in the previous section, Thamm et al.[35] observed that their isolated hydroperoxymethyl formate (HPMF) readily decomposed into formic acid anhydride (FAA; HC(═O)OC(═O)H), formic acid, and CH_2═O. The potential energy surface for HPMF dehydration is plotted in Figure 5. We found two different transition states leading to FAA and H_2O. Geometries for these two transition states are shown in Figure 6a and 6b, which are connected to the conformations of HPMF illustrated in Figures 4b and 4a, respectively. b-TS3 is lower in energy than b-TS3′, with enthalpies of ΔH_{298}(b-TS3) = −19.0 kcal/mol and ΔH_{298}(b-TS3′) = −16.4 kcal/mol with respect to O_2 and

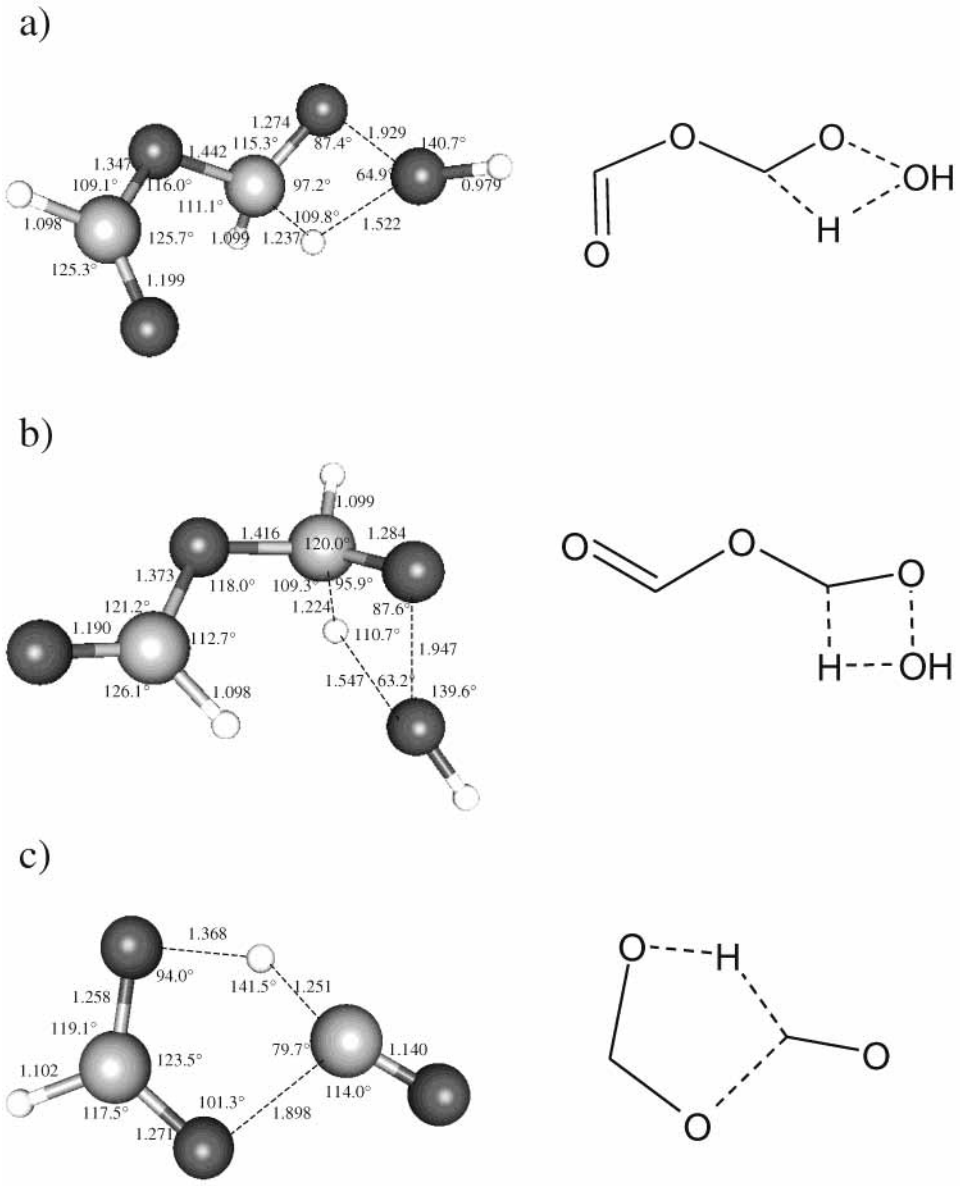

Figure 6. Alternate path leading to FAA and ·OH. (a) b-TS3 connects HPMF [sp,ap] with FAA and H_2O, and (b) b-TS3′ connects HPMF [ap,ap] with FAA and H_2O. (c) b-TS4: connects FAA [sp,ap] with HC(═O)OH and CO.

·CH_2OCH_2OOH. The activation energies are E_a(b-TS3) = 49.4 kcal/mol and E_a(b-TS3′) = 52.0 kcal/mol relative to HPMF. The transition state from HPMF to H_2O and FAA was calculated previously at the DFT-B3LYP/6-31G(d,p) level of theory by Aplincourt and Ruiz-López.[34] Our b-TS3 geometry (see Figure 6a) is almost identical to their transition state geometry for HPMF dehydration. This b-TS3 transition state, however, is about 6−7 kcal/mol higher than that for the path leading to the direct formation of ·OH, HĊ═O, and HC(═O)OH discussed above and therefore appears unfavorable. However, an evaluation of kinetics and dynamics will be required to determine whether HPMF dehydration could occur at temperature and pressure conditions pertinent to a diesel engine. Aplincourt and Ruiz-López[34] have suggested that an ancillary formic acid molecule could aid the dehydration of HPMF. They reported a 21.6 kcal/mol reduction in the barrier to HPMF dehydration in formic-acid-assisted dehydration compared to self-dehydration of HPMF (at the DFT-B3LYP/6-31G(d,p) level of theory). This barrier is 12.7 kcal/mol lower than b-TS2. Thus secondary chemistry due to the presence of reactive species such as formic acid (present during synthesis of HPMF) may explain the propensity of HPMF toward dehydration in the experiments of Thamm et al. at standard temperature and pressure. Under extreme temperature and pressure conditions, however, it is unclear whether dehydration will be the primary route for HPMF decomposition, especially when formic acid is not present initially in the DME combustion system.

Finally, the FAA resulting from HPMF decomposition, like HPMF itself, is not thermally stable and readily forms HC(═O)OH and CO. The transition state (b-TS4) for FAA decomposition into formic acid and CO (see Figures 5 and 6) involves an intramolecular hydrogen transfer, with a barrier (at 298 K) of E_a = 28.0 kcal/mol.[34] Again, three possible conformations for FAA exist (similar to the three described for HPMF), shown in Figures 7a−c. In order for a hydrogen transfer to take place, FAA must possess the conformation of Figure 7c, which, incidentally, has the lowest energy of the three conformations (by 3.4 kcal/mol). This is likely due to the O·· ·H attraction in the third FAA conformation. Both b-TS3 and b-TS3′ lead to the lowest-energy FAA conformation shown in Figure 7c, which then in turn is the reactive conformation to surmount b-TS4 to form formic acid and CO.

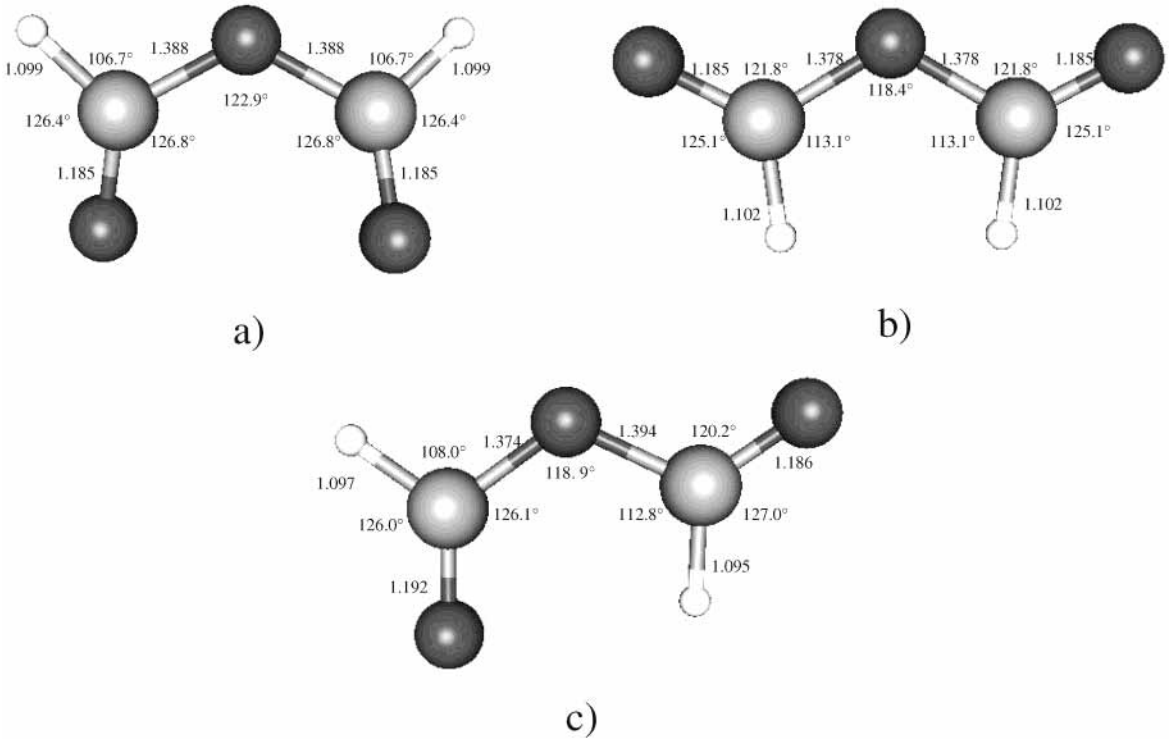

Figure 7. Formic acid anhydride (FAA) conformation defined by the O═C−O−C torsion angles: (a) synperiplanar, synperiplanar [sp,sp], (b) antiplanar, antiplanar [ap,ap], and (c) synperiplanar, antiplanar [sp,ap].

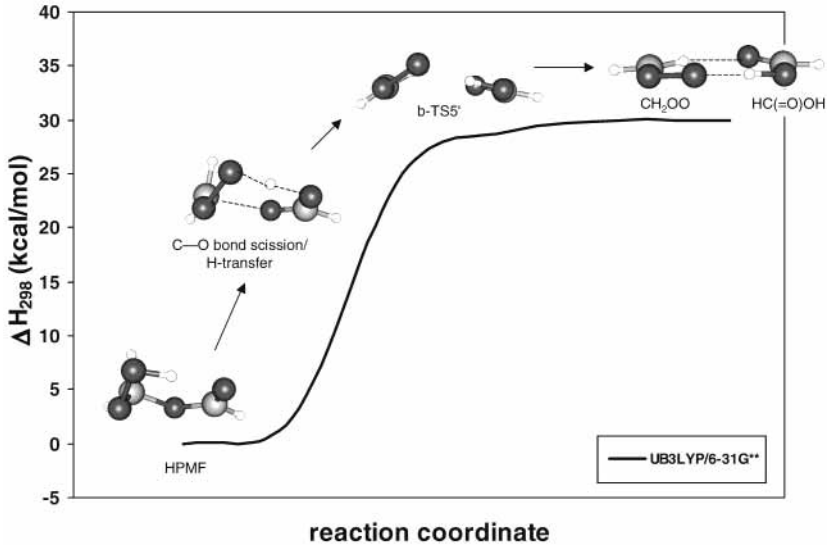

Figure 8. Path for the formation of the formic acid and carbonyl oxide hydrogen-bonded adduct. Note the CH_2OO fragment rotation with respect to the HC(═O)OH fragment. C−O bond scission/H-transfer appears to be barrierless.

2. Formation of the Criegee Intermediate (carbonyl oxide) and Formic Acid. Another possible decomposition of HPMF, with a transition state (b-TS5) comparable in energy to b-TS2, leads to carbonyl oxide (·CH_2OO·) and formic acid (Figure 8). b-TS5 involves a transfer of HPMF's peroxide hydrogen to the ether oxygen (see Figure 9a) with a concerted C−O cleavage to form CH_2OO and formic acid. b-TS5 lies below ·CH_2OCH_2-OOH and O_2 by $\Delta H_{298} = -25.0$ kcal/mol. The activation energy (at 298 K) with respect to the lowest-energy $HOOCH_2OC(=O)H$ conformer (Figure 4b) is $E_a = 43.4$ kcal/mol (at 298 K), which is on par with that of b-TS2 along the branching path ($E_a^{b-TS2} = 43.7$ kcal/mol), given that 0.3 kcal/mol is well within the uncertainty of the theory used here. Like b-TS2, the high-pressure A-factor of b-TS5 is in the $10^{14}-10^{15}$ s^{-1} range.[29] b-TS5 is only 1−2 kcal/mol above the products, and hence, according to Hammond's postulate, its structure is very product-like. Thus production of ·CH_2OO· and HC(═O)OH appears very competitive with the branching path leading directly to HC(═O)OH, HĊO, and the second ·OH needed for chain-branching.

An alternative transition state to b-TS5 leading to ·CH_2OO· and HC(═O)OH can occur when the peroxide hydrogen of HPMF is transferred to the formaldehyde oxygen. We would expect that the barrier would be lower due to the reduced ring strain (from five to seven atoms). We found an unconventional transition state (b-TS5′) directly leading to a cyclical hydrogen-bonded complex (Figure 9b). The imaginary frequency of this transition state structure along the reaction coordinate (55.7*i* cm^{-1}) is consistent with a torsional rather than a stretching mode. DVV does indeed show that this saddle-point connects

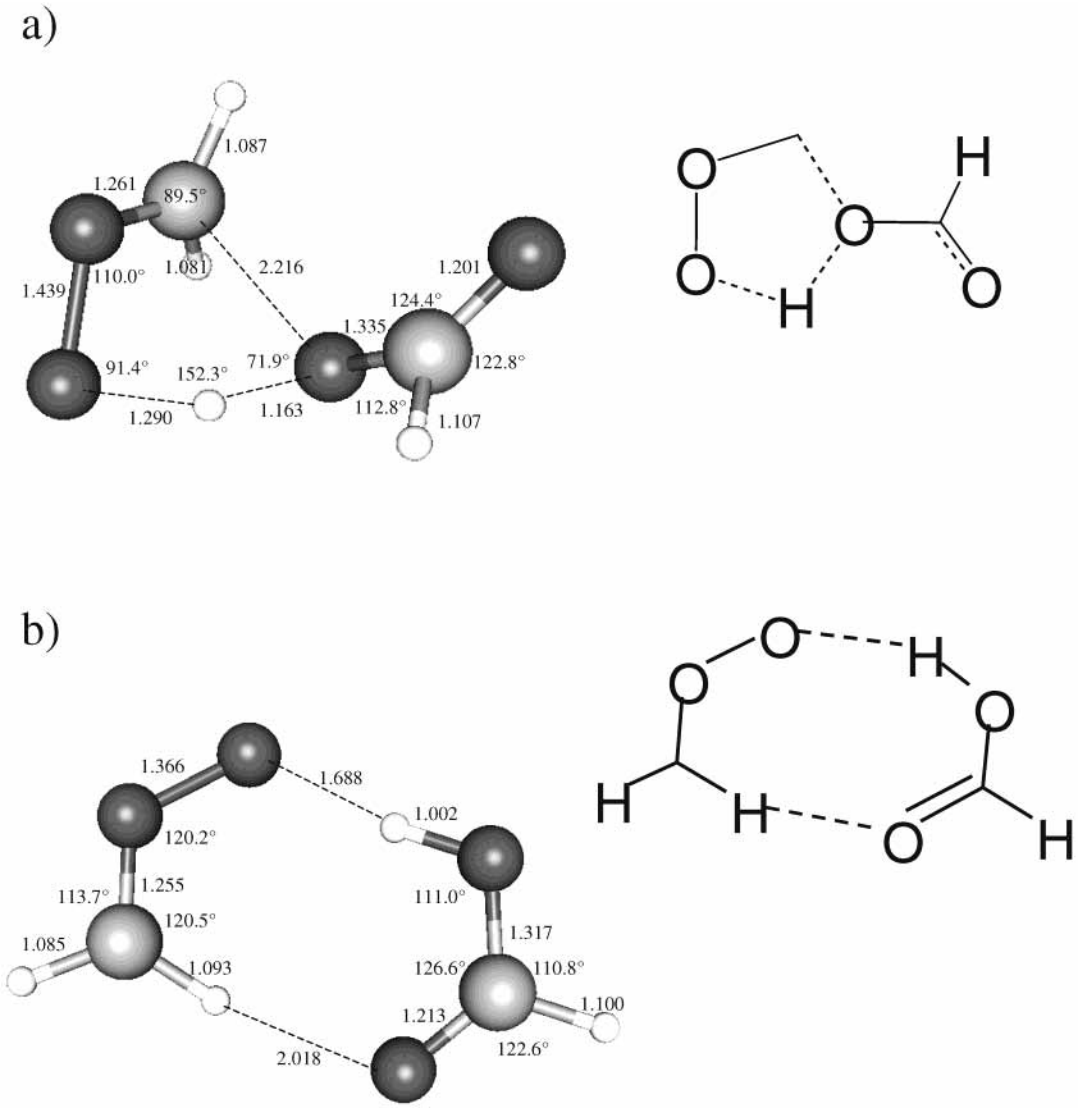

Figure 9. (a) b-TS5: connects HPMF [sp,ap] to carbonyl oxide (·CH_2OO·) and formic acid (HC(═O)OH). (b) Formic acid and carbonyl oxide adduct.

HPMF [sp,sp] and $CH_2OO\cdots HC(=O)OH$. This transition state has an enthalpy identical to the $HC(=O)OH\cdots CH_2OO$ adduct (note that the barrier to addition of CH_2OO and HC(═O)OH is only 1−2 kcal/mol according to b-TS5 in the reverse direction; b-TS5 is more strained than what we find here). Figure 8 depicts the rather flat path from HPMF to the Criegee intermediate/formic acid complex. Both CH_2OO and its isomer HC(═O)OH have C_s symmetry, where CH_2OO has a π-electronic structure analogous to that of ozone (a four-electron-in-three-orbital π-system).[40] The ground state of ·CH_2OO· is an open-shell singlet, as in ozone. HPMF is formed when the mirror planes of CH_2OO and HC(═O)OH are perpendicular (intermolecular π-orbital overlap in the adduct is maximized), and the Criegee intermediate/formic acid hydrogen-bonded complex is formed when the mirror planes of CH_2OO and HC(═O)OH are parallel (intermolecular π-orbital overlap is minimized). The enthalpy of the $HC(=O)OH\cdots CH_2OO$ adduct is $\Delta_{rxn}H_{298} = 28.7$ kcal/mol with respect to the lowest-energy HPMF conformation, ∼10 kcal/mol lower than the enthalpies required to break the O−O bond in HPMF and surmount the b-TS2 or b-TS5 transition state barriers, but the high-pressure A-factor is slightly lower than those for b-TS2 and b-TS5 (about 10^{14} s^{-1}).[29] The isolated ·CH_2OO· and HC(═O)OH products, however, are 13−14 kcal/mol higher in energy than the $CH_2OO\cdots HC(=O)OH$ adduct. This is most likely a reflection of the amount of energy in the O−H···O and C−H···O hydrogen bonds binding the ·CH_2OO· and HC(═O)OH fragments together (see Figure 9b). This hydrogen bonding may be somewhat overestimated in our DFT work; hybrid density functionals such as B3LYP are known to overestimate proton affinities and underestimate energy barriers for proton transfer.[16,41−43]

The ·CH_2OO· biradical, or carbonyl oxide, is a well-known postulated species in the field of atmospheric chemistry. This biradical is known as the "Criegee" intermediate of ethylene ozonolysis.[44] As far as we know, this is the first study that has considered carbonyl oxide in the context of fuel autoignition in internal combustion engines. As a result, unfortunately, all experiments involving ·CH_2OO· have been performed at standard temperature (298 K) and pressure (1 atm). The Criegee intermediate has never been observed spectroscopically under atmospheric conditions and has been deduced only through product analysis.[45] As noted above, HPMF itself was synthesized through the addition of the HC(═O)OH to the elusive Criegee intermediate in ethyl vinyl ether ozonolysis.[35] ·OH production from the Criegee intermediate has been measured indirectly (by detailed kinetics measurements or the disappearance of ·OH scavenging molecules) in ethylene ozonolysis;[45−47] therefore, decomposition of the Criegee singlet biradical in principle can

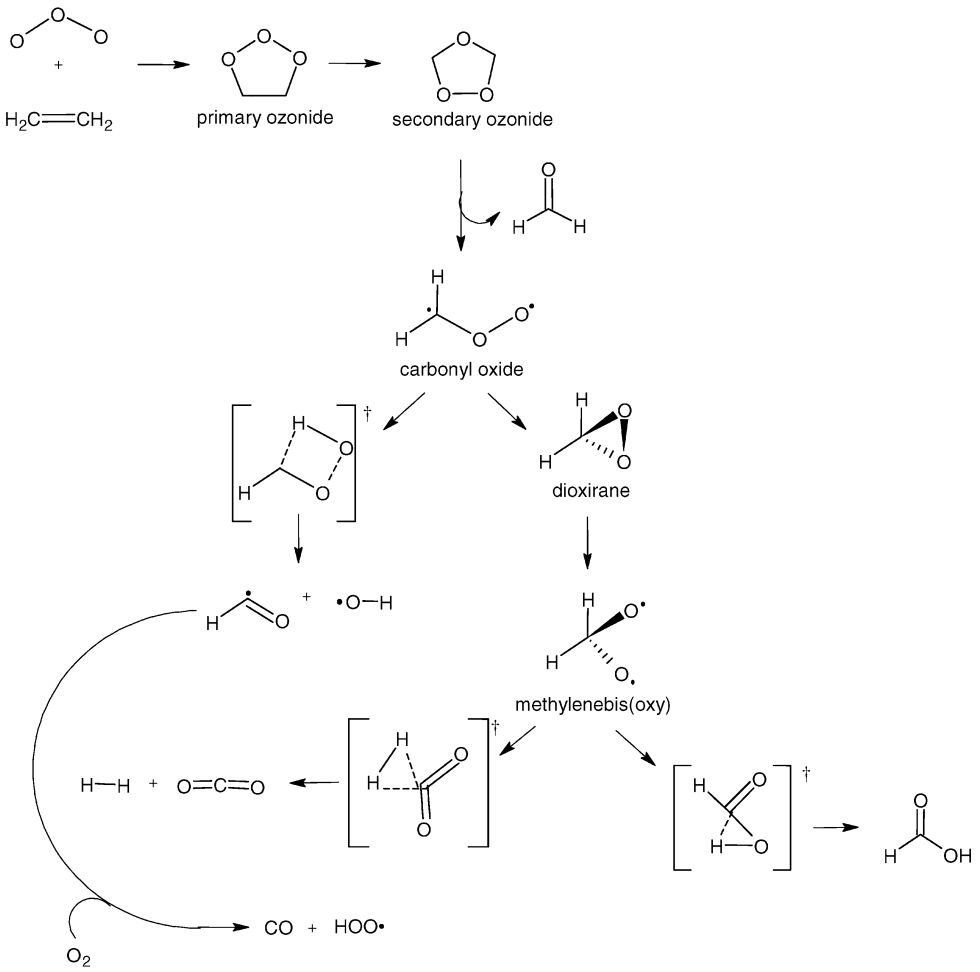

Figure 10. Schematic diagram of Criegee intermediate (carbonyl oxide) decomposition pathways.

lead to the formation of the second ·OH necessary for chain-branching. The yield of ·OH from vibrationally excited CH_2OO*, however, has been estimated to be only 8−22% at standard temperature and pressure.[46−50] Fenske et al.[47] have shown that ·OH yield decreases with increasing pressure (especially with an excellent energy absorber like SF_6). This indicates that collisionally stabilized $\cdot CH_2OO\cdot$ is unlikely to decompose into ·OH and HĊO. Thus, this is the least likely decomposition scenario for $\cdot CH_2OO\cdot$ in a high-pressure environment.

Gutbrod et al.[51] studied possible decomposition paths for vibrationally excited CH_2OO* with high-level ab initio calculations (CCSD(T)) and have shown that the barrier to a concerted elimination of ·OH from CH_2OO* is 13 kcal/mol higher than that for isomerization to dioxirane. Figure 10 shows the proposed decomposition pathways of the ethylene Criegee intermediate.[51] The O−O bond in dioxirane then breaks to form methylenebis-(oxy), which either decomposes to form CO_2 and H_2 or (most likely) rearranges to form vibrationally excited formic acid. The decomposition of vibrationally excited HC(═O)OH most likely leads to H_2O + CO and H_2 + CO_2, with the dehydration of formic acid being much more favorable than the decarboxylation of formic acid.[51−56]

On the other hand, if $\cdot CH_2OO\cdot$ has the chance to thermalize through collisions, Criegee intermediate scavengers such as CH_2O[45] and H_2O[57] can possibly facilitate bimolecular production of ·OH. Both of these scavengers are readily available from the product path of the chain-propagating step (for CH_2═O) and the dehydration of HPMF (for H_2O). Interaction of the Criegee intermediate with CH_2═O is most likely, since the

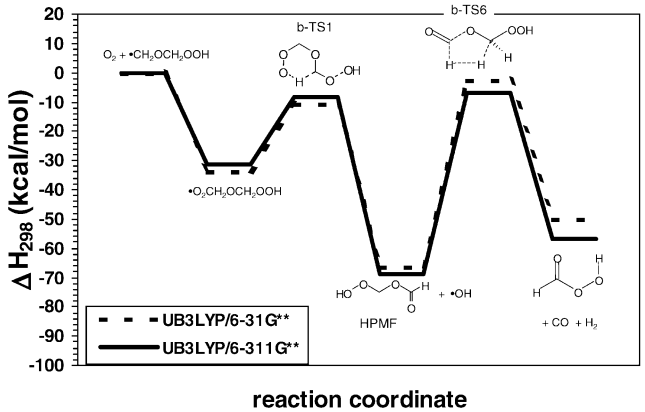

Figure 11. Potential energy surface of path leading to peroxyformic acid, CO, and H_2.

chain-branching path from $\cdot CH_2OCH_2OOH$ is competing with the decomposition of $\cdot CH_2OCH_2OOH$ to CH_2═O and ·OH. Neeb et al.[46,58] have performed kinetic isotope experiments of the $\cdot CH_2OO\cdot$ reaction with $^{13}CH_2$═O. They observed a substantial amount of $H^{13}C$(═O)OH and deduced that the following reaction was occurring:

$$\cdot CH_2OO\cdot + {}^{13}CH_2{=}O \rightarrow CH_2{=}O + H^{13}C(=O)OH \quad (13)$$

They also saw a substantial amount of ^{13}CO. They propose that the excess $^{13}CH_2$═O added to the system combines to form the secondary ozonide (see Figure 10), which can decompose into

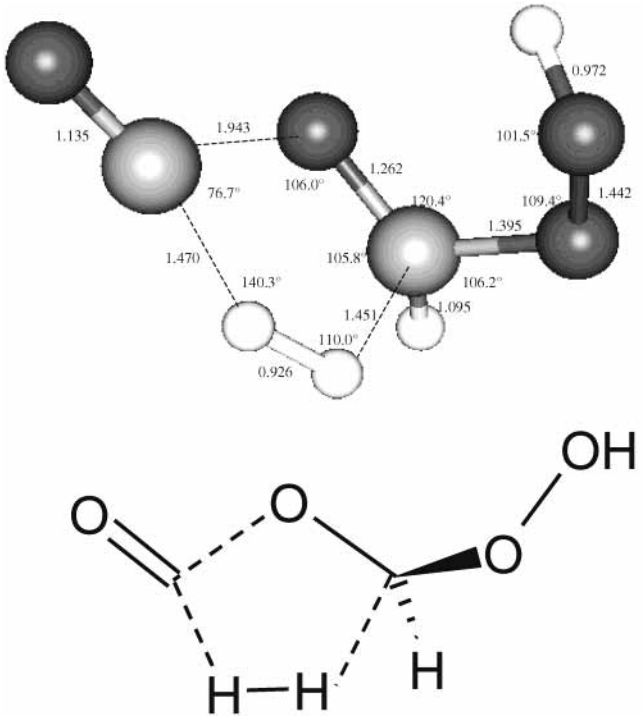

Figure 12. b-TS6: connects HPMF [ap,ap] to HC(═O)OOH, H_2, and CO.

CH_2═O and $^{13}CH_2OO$. With a new distribution of internal energy, the ·$^{13}CH_2OO$· can undergo the various branches of decomposition illustrated in Figure 10 (one of these leading to H^{13}Ċ═O and ·OH). They also propose that ·CH_2OO· can remove a hydrogen from the ^{13}C-labeled formaldehyde to form ·CH_2OOH and H^{13}Ċ═O. As noted in chain propagation, Part I,[3] ·CH_2OOH promptly forms CH_2═O + ·OH.

Except for the path for bond scission, the three mechanisms for HPMF decomposition discussed above (direct formation of HC(═O)OH, HĊO, and ·OH from HPMF, dehydration of HPMF, and formation of ·CH_2OO· and HC(═O)OH from HPMF) definitely lead to the production of formic acid. Since formic acid is a major product in the low-temperature combustion of DME,[9,11] these paths are the most likely paths for HPMF decomposition. Further work including pressure and temperature effects will be needed to determine which of these mechanisms is the most likely route for HPMF decomposition.

3. Formation of H_2, CO, and Peroxyformic Acid. Though H_2 has been detected only in high-temperature experiments, HPMF can possibly decompose into H_2, CO, and peroxyformic acid.[14] We searched for a possible path leading to H_2 formation. This proceeds through b-TS6 (see Figures 11 and 12). The enthalpy with respect to O_2 and ·CH_2OCH_2OOH for b-TS6 is $\Delta H_{298} = -5.4$ kcal/mol. The activation energy with respect to the lowest-energy HPMF conformation is $E_a = 63.0$ kcal/mol, which is much higher than the transition states from HPMF discussed earlier. b-TS6, however, is still lower in energy than O_2 and ·CH_2OCH_2OOH. Thus, in principle, H_2, CO, and HC(═O)OOH production is possible.

Peroxyformic acid is not a product that has been suggested for combustion reactions: it is an excellent oxidizer used in the epoxidation of alkenes.[59] Literature on peroxyacids describes their solution phase properties, but the gas-phase literature is nonexistent; a solution containing peroxyformic acid can be prepared with a solution of formic acid. Equilibrium is established between the formic acid and hydrogen peroxide reagents and the peroxyformic acid and water products.[59] Thus

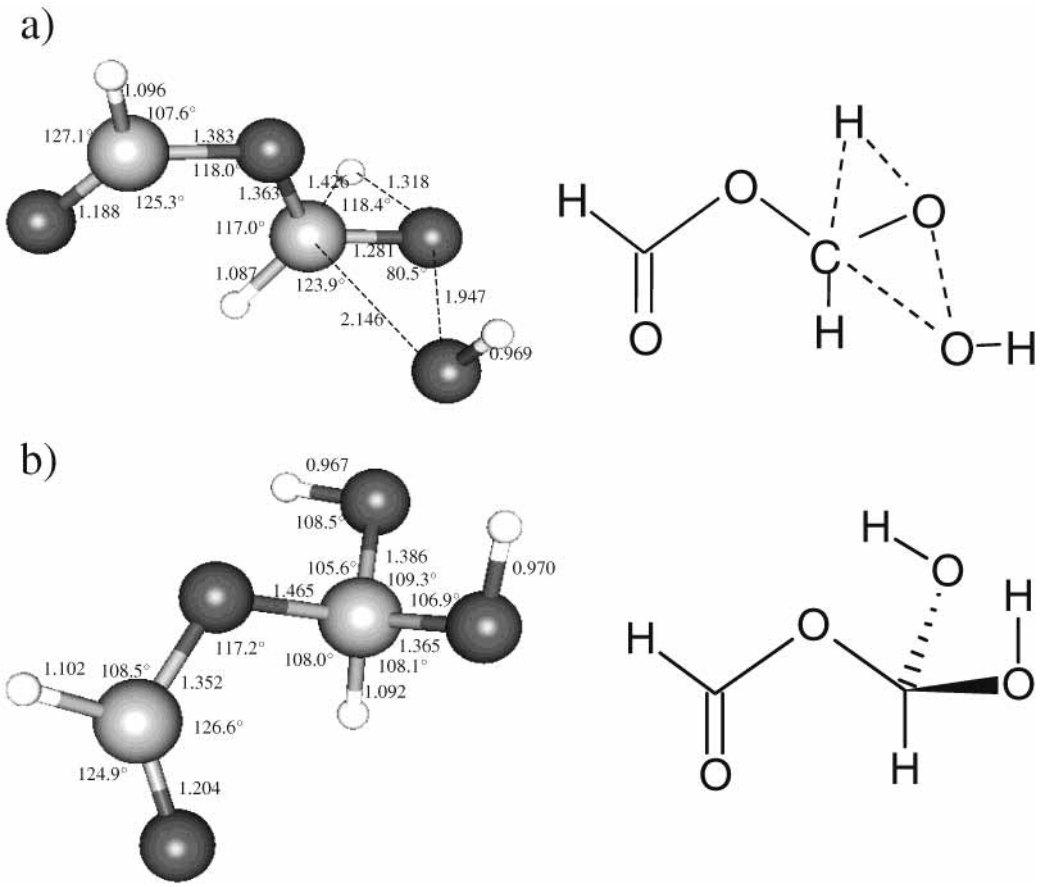

Figure 13. (a) b-TS7: connects HPMF [sp,ap] to dihydroxymethyl formate (DHMF). (b) Dihydroxymethyl formate (DHMF).

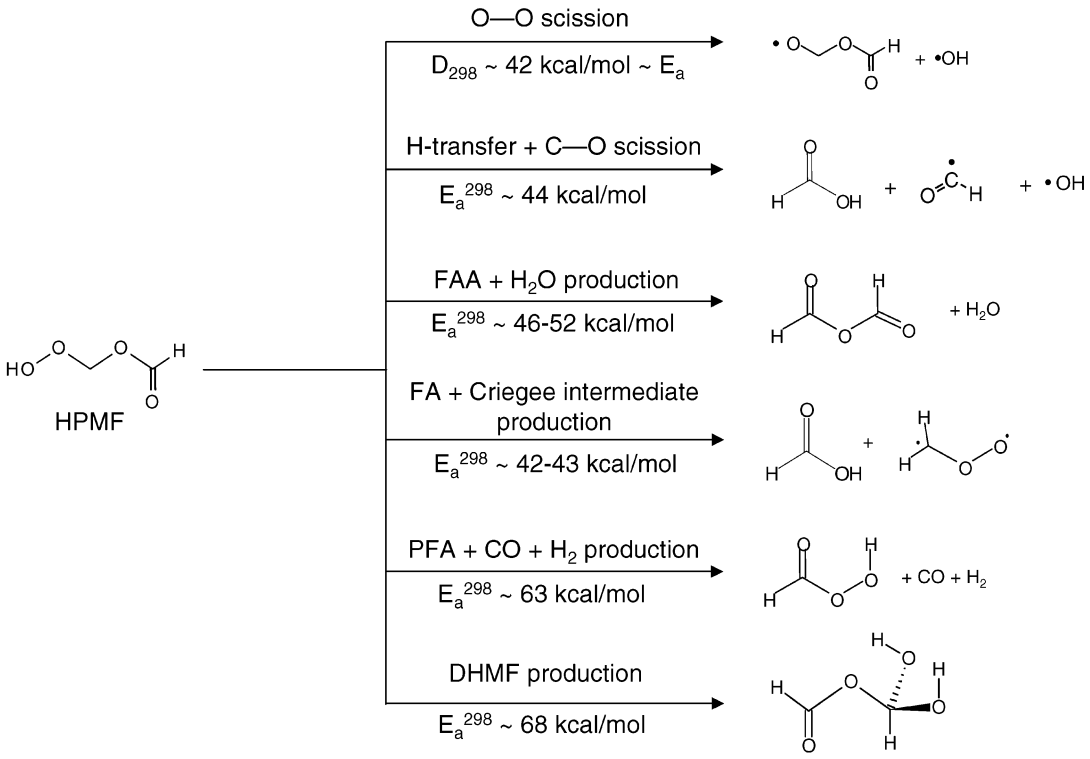

Figure 14. Schematic summary of the activation energies needed to form the products considered in this work.

it is feasible that peroxyformic acid and H_2O may combine in the gas phase to produce formic acid and hydrogen peroxide. The origin of the water vapor for this reaction might be available from the dehydration of HPMF, which is a competing reaction in its decomposition. Therefore, peroxyformic acid−H_2O reactions at low-to-intermediate temperatures might contribute to the hydrogen peroxide pool required for high-temperature, non-chain-branching DME oxidation. Alternatively, peroxyformic acid can react with ambient formaldehyde to form two HC(═O)OH.[59] Though formic acid potentially can be formed, the potential energy barrier is much higher than the other barriers discussed previously and, therefore, will not be a likely path for HPMF decomposition.

4. Formation of Dihydroxymethyl Formate ((HO)$_2$CHO(C═O)H). Last, we have found an HPMF decomposition path leading to a highly stable geminal diol/aldehyde product, dihydroxymethyl formate (DHMF). The transition state (b-TS7) may lie slightly below with $\cdot CH_2OCH_2OOH$ and O_2, with $\Delta H_{298} = -1.6$ kcal/mol. We concluded that this is the least likely fate for $HOOCH_2OC(=O)H$, since the transition state barrier has almost the same enthalpy as the branching reactants $\cdot CH_2OCH_2OOH$ and O_2. b-TS7, depicted in Figure 13a, involves a transfer of the OH group in $HOOCH_2OC(=O)H$ to the saturated carbon and a simultaneous transfer of the one of the hydrogen atoms on the saturated carbon to the oxygen bonded to the saturated carbon. Despite the high activation energy, we note that the DHMF product (with one geminal diol end and one aldehyde end; see Figure 13b) is the most stable product of all the products and intermediates considered here.

IV. Summary and Conclusions

In this work, we examined an oxidation mechanism for dimethyl ether (DME) low-temperature autoignition (300−1000 K). This mechanism is analogous to the one used to explain alkane autoignition. This mechanism is comprised of three main steps: chain initiation, followed by chain propagation, and then chain branching. The Lindemann-type reaction in the chain-propagation step is responsible for the shift from low-temperature oxidation (where chain-branching leads to weakly explosive combustion) to high-temperature oxidation (where a non-chain-branching mechanism, such as HO−OH bond cleavage, may drive explosive combustion). This was discussed in Part I.[3]

Up until the creation of hydroperoxymethyl formate (HPMF), the chain-branching path is unambiguous; O_2 adds to $\cdot CH_2OCH_2OOH$, and the resulting $\cdot OOCH_2OCH_2OOH$ can either dissociate back into $O_2 + \cdot CH_2OCH_2OOH$, stabilize via collisions, or undergo a hydrogen-transfer isomerization to form $HOOCH_2O\dot{C}HOOH$. We find that $HOOCH_2O\dot{C}HOOH$ readily dissociates into $HOOCH_2OC(=O)H$ (HPMF) and the first ·OH needed for chain-branching. HPMF has many possible decomposition pathways, as summarized in Figure 14. Only one of these pathways leads to direct formation of the second ·OH necessary for chain-branching, along with formic acid (experimentally observed in DME combustion[9,11]) and $H\dot{C}{=}O$. We have located the transition state (b-TS2) for this path ($E_a = 44$ kcal/mol), which was originally proposed by Curran et al.[11] These latter authors, however, favor the O−O scission path leading to the formation of $\cdot OCH_2OC(=O)H$ and ·OH, arguing that the A-factor for this reaction is likely to be higher than that for the direct path to ·OH via H-transfer, potentially resulting in a higher rate constant than the path involving b-TS2. While O−O scission may be 2 kcal/mol more favorable than the direct path to ·OH via H-transfer and may have a higher A-factor, only a variational transition state theory calculation (accounting for the intrinsic barrier of this reaction) can show if the O−O scission is actually a more favorable kinetic path compared with the path through b-TS2.

At atmospheric temperature and pressure, Thamm et al.[35] observed that the decomposition products for HPMF (formed via ethyl vinyl ether ozonolysis) are formic acid anhydride, formic acid, and $CH_2{=}O$.[35] According to our calculations (in

agreement with those of Aplincourt and Ruiz-López[34]), dehydration is not as energetically favorable as the mechanism proposed by Curran et al.[11] However, Aplincourt and Ruiz-López[34,60] predicted that the addition of an ancillary formic acid to HPMF decreases the barrier to dehydration by 21.6 kcal/mol (E_a = 33.9 kcal/mol). This is lower than any other transition state we have found and may explain why Thamm et al.[35] observed dehydration products (in the presence of excess formic acid). To the extent formic acid is present, this may drive dehydration of HPMF, producing water and formic acid anhydride.

In ethylene ozonolysis, HPMF is formed by the addition of the Criegee intermediate, ·CH_2OO·, to formic acid. *We suggest here that the Criegee intermediate may be formed in the course of dimethyl ether (DME) combustion.* Two transition states leading from HPMF to the Criegee intermediate itself (·CH_2OO·) and HC(═O)OH were found. One transition state (b-TS5′) is higher than the other (b-TS5) by ∼15 kcal/mol (due to higher ring strain). Both of these transition states are lower than the transition state leading to the direct formation of ·OH, and, therefore, may provide a more favorable HPMF decomposition mechanism. HPMF also may simply dissociate into ·OH and ·OCH_2C(═O)H; the cost to cleave the O−O bond in HPMF is slightly below the energy to surmount b-TS2 and b-TS5. HPMF may also dissociate into H_2, CO, and HC(═O)OOH; the enthalpy of b-TS6 is below that of b-TS1, and, therefore, the path is feasible. The subsequent decomposition and reactions of HC(═O)OOH in the gas phase are even less characterized than the intermediates involved in ethylene ozonolysis. Finally, the isomerization of HPMF to DHMF has the highest kinetic barrier, despite DHMF's high stability.

From the energetics alone, the path leading to direct formation of ·OH (along with production of HĊ═O and formic acid), the path involving O−O bond scission in HPMF, and the path leading to the Criegee intermediate (·CH_2OO·) and formic acid are the most favorable mechanisms for HPMF decomposition (all of which may lead to the second ·OH required for possible explosive combustion). However, we emphasize that only a very basic unimolecular mechanism for the low-temperature autoignition of DME with the occasional bimolecular reaction with O_2 at the beginning of chain-propagation[3] and chain-branching has been considered here. The kinetics of DME autoignition may be much more complex than this simplified chain-branching scheme described here, especially with this unexpected overlap with olefin ozonolysis reactions. Many factors such as temperature, pressure, and relative concentrations will greatly influence changes in kinetics. Further analysis is needed to determine the extent that these factors influence DME combustion.

Acknowledgment. A. A. and E.A.C. thank Mr. J. J. Szente and Drs. E. W. Kaiser and W. F. Schneider for their helpful conversation. Funding for this work was provided by the Ford Motor Company.

References and Notes

(1) U. S. Environmental Protection Agency, *Federal Register* **2001**, *66*, 5001−5050 Part V.; 40 CFR Parts 69, 80 and 86; [AMS−FRL-6923−7]; RIN 2060-AI69.

(2) Sorenson, S. C. *Trans. ASME* **2001**, *123*, 652−657 and references therein.

(3) Andersen, A.; Carter, E. A. *Isr. J. Chem.* **2002**, *42*, 245−260.

(4) Glassman, I. *Combustion;* Academic Press: San Diego, 3rd ed.; 1996 Chapter 3.

(5) Semenov, N. *Chemical Kinetics and Chain Reactions*; Oxford: London, 1935.

(6) Sehested, J.; Møgelberg, T.; Wallington, T. J.; Kaiser, E. W.; Nielsen, O. J. *J. Phys. Chem.* **1996**, *100*, 17218−17225.

(7) Maricq, M. M.; Szente, J. J.; Hybl, J. D. *J. Phys. Chem. A* **1997**, *101*, 5155−5167.

(8) Pfahl, U.; Fieweger, K.; Adomeit, G. Self-ignition of diesel-relevant hydrocarbon-air mixtures under conditions. In *Twenty-Sixth Symposium (International) on Combustion*; The Combustion Institute: Pittsburgh, 1996 pp. 781−789.

(9) Liu, I.; Cant, N. W.; Bromly, J. H.; Barnes, F. J.; Nelson, P. F.; Haynes, B. S. *Chemosphere* **2001**, *42*, 583−589.

(10) Curran, H. J.; Pitz, W. J.; Westbrook, C. K.; Dagaut, P.; Boettner, J.-C.; Cathonnet, M. *Int. J. Chem. Kinet.* **1998**, *30*, 229−241.

(11) Curran, H. J.; Fischer, S. L.; Dryer, F. L. *Int. J. Chem. Kinet.* **2000**, *32*, 741−759.

(12) Westbrook, C. K. *Chem. Ind.* **1992**, *100*, 562−566.

(13) Heywood, J. B. *Internal Combustion Engine Fundamentals;* McGraw-Hill: New York, 1988 Chapter 10.

(14) Dagaut, P.; Boettner, J.-C.; Cathonnet, M. Chemical kinetics study of dimethyl ether oxidation in a jet stirred reactor from 1 to 10 atm: experiments and kinetics modeling. In *Twenty-Sixth Symposium (International) on Combustion*; The Combustion Institute: Pittsburgh, 1996 pp 627−632.

(15) Sehested, J.; Sehested, K.; Platz, J.; Egsgaard, H.; Nielsen, O. J. *Int. J. Chem. Kinet.* **1997**, *29*, 627−636.

(16) Becke, A. D. *J. Chem. Phys.* **1993**, *98*, 5648−5652.

(17) Becke, A. D. *Phys. Rev. A* **1988**, *38*, 3098.

(18) Lee, C.; Yang, W.; Parr, R. G. *Phys. Rev. B* **1988**, *38*, 785−789.

(19) Miehlich, B.; Savin, A.; Stoll, H.; Preuss, H. *Chem. Phys. Lett.* **1989**, *157*, 200−206.

(20) Stephens, P. J.; Devlin, F. J.; Chabalowski, C. F.; Frisch, M. J. *J. Phys. Chem.* **1994**, *98*, 11623−11627.

(21) Jaguar v4.1, Schrödinger, Inc., Portland, OR, 2000.

(22) Hehre, W. J.; Ditchfield, R.; Pople, J. A. *J. Chem. Phys.* **1972**, *56*, 2257−2261.

(23) Hariharan, P.; Pople, J. *Theor. Chim. Acta* **1973**, *28*, 213.

(24) Francl, M.; Petro, W.; Hehre, W. J.; Binkley, J.; Gordon, M.; Defrees, D.; Pople, J. *J. Chem. Phys.* **1982**, *77*, 3654−3665.

(25) Krishnan, R.; Binkley, J. S.; Seeger, R.; Pople, J. A. *J. Chem. Phys.* **1980**, *72*, 650−654.

(26) Ignatyev, I. S.; Xie, Y.; Allen, W. D.; Schaefer, H. F., III. *J. Chem. Phys.* **1997**, *107*, 141−155.

(27) Rienstra-Kiracofe, J. C.; Allen, W. D.; Schaefer, H. F., III. *J. Phys. Chem. A* **2000**, *104*, 9823−9840.

(28) Hratchian, H. P.; Schlegel, H. B. *J. Phys. Chem. A* **2002**, *106*, 165−169.

(29) Andersen, A.; Carter, E. A., to be published.

(30) Swope, W. C.; Andersen, H. C. *J. Chem. Phys.* **1982**, *76*, 637.

(31) da Silva, A. J. R.; Carter, E. A., unpublished work.

(32) Knyazev, V. D.; Slagle, I. R. *J. Phys. Chem. A* **1998**, *102*, 1770−1778.

(33) Fischer, S. L.; Dryer, F. L.; Curran, H. J. *Int. J. Chem. Kinet.* **2000**, *32*, 713−740.

(34) Aplincourt, P.; Ruiz-López, M. F. *J. Phys. Chem. A* **2000**, *104*, 380−388.

(35) Thamm, J.; Wolff, S.; Becker, K. H. *Chem. Phys. Lett.* **1996**, *258*, 155−158.

(36) Gilbert, R. G.; Smith, S. C. *Theory of Unimolecular and Recombination Reactions;* Blackwell Scientific Publications: Oxford, 1990.

(37) Baulch, D. L.; Cobos, C. J.; Cox, R. A.; Frak, P.; Hayman, G.; Just, T.; Kerr, J. A.; Murrells, T.; Pilling, M. J.; Troe, J.; Walker, R. W.; Warnatz, J. *J. Phys. Chem. Ref. Data* **1994**, *23*, 847−1033.

(38) Sahetchian, K. A.; Rigny, R.; Tardieu de Maleissye, J.; Batt, L.; Mathews, M. A. S. *Twenty-Fourth Symposium (International) on Combustion* **1992**, *24*, 637−643.

(39) Clifford, E. P.; Wenthold, P. G.; Gareyev, R.; Lineberger, W. C.; DePuy, C. H.; Bierbaum, V. M.; Ellison, G. B. *J. Chem. Phys.* **1998**, *109*, 10293.

(40) Goddard, W. A., III.; Dunning, T. H., Jr.; Hunt, W. J.; Hay, P. J. *Acc. Chem. Res.* **1973**, *6*, 368.

(41) Ben-Nun, M.; Martinez, T. J. *J. Phys. Chem. A* **1999**, *103*, 6055−6059.

(42) Lee, S.; Cox, H.; Goddard, W. A., III.; Beauchamp, J. L. *J. Am. Chem. Soc.* **2000**, *122*, 9201−9205.

(43) Ferreiro, M. L.; Rodríguez-Otero, J. *J. Mol. Struct. (THEOCHEM)* **2001**, *542*, 63−77.

(44) Criegee, R. *Angew. Chem., Int. Ed. Engl.* **1975**, *14*, 745−751.

(45) Horie, O.; Moortgat, G. K. *Acc. Chem. Res.* **1998**, *31*, 387−396.

(46) Neeb, P.; Horie, O.; Moortgat, G. K. *J. Phys. Chem. A* **1998**, *102*, 6778−6785.

(47) Fenske, J. D.; Hasson, A. S.; Paulson, S. E.; Kuwata, K. T.; Ho, A.; Houk, K. N. *J. Phys. Chem. A* **2000**, *104*, 7821−7833.

(48) Atkinson, R. *J. Chem. Phys. Ref. Data* **1997**, *26*, 215−290.

(49) Rickard, A. R.; Johnson, D.; McGill, C. D.; Marston, G. *J. Phys. Chem. A* **1999**, *103*, 7656−7664.

(50) Gutbrod, R.; Meyer, S.; Rahman, M. M.; Schindler, R. N. *Int. J. Chem. Kinet.* **1997**, *29*, 717−723.
(51) Gutbrod, R.; Kraka, E.; Schindler, R. N.; Cremer, D. *J. Am. Chem. Soc.* **1997**, *119*, 7330−7342.
(52) Francisco, J. S. *J. Chem. Phys.* **1992**, *96*, 1167−1175.
(53) Goddard, J. D.; Yamaguchi, Y.; Schaefer, H. F., III. *J. Chem. Phys.* **1992**, *96*, 1158−1166.
(54) Cremer, D.; Kraka, E.; Szalay, P. G. *Chem. Phys. Lett.* **1998**, *292*, 97−109.
(55) Su, H.; Mao, W.; Kong, F. *Chem. Phys. Lett.* **2000**, *322*, 21−26.
(56) Fang, D.-C.; Fu, X.-Y. *J. Phys. Chem. A* **2002**, *106*, 2988−2993.
(57) Paulson, S. E.; Flagan, R. C.; Seinfeld, J. H. *Int. J. Chem. Kinet.* **1992**, *24*, 103−125.
(58) Neeb, P.; Moortgat, G. K. *J. Phys. Chem. A* **1999**, *103*, 9003−9012.
(59) Davies, A. G. *Organic Peroxides;* Butterworth: London, 1961.
(60) Aplincourt, P.; Ruiz-López, M. F. *J. Am. Chem. Soc.* **2000**, *122*, 8990−8997.
(61) A list of optimized geometries and harmonic vibrational frequencies (calculated with the 6-311G** basis set) for each species considered in this study is available upon request from the corresponding author.